Neurochemistry International 180 (2024) 105854

Contents lists available at ScienceDirect

Neurochemistry International

journal homepage: www.elsevier.com/locate/neuint

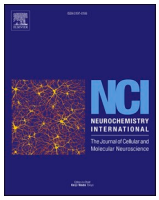

Generation and characterization of cortical organoids from iPSC-derived dental pulp stem cells using traditional and innovative approaches

André Luíz Teles e Silva [a,1], Bruno Yukio Yokota-Moreno [a,1], Mariana Silva Branquinho [a], Geisa Rodrigues Salles [b], Thiago Cattuzo de Souza [a], Ronald Almeida de Carvalho [c], Gabriel Batista [c], Elisa Varella Branco [d], Karina Griesi-Oliveira [a], Maria Rita Passos Bueno [d], Marimélia Aparecida Porcionatto [b], Roberto Hirochi Herai [c], Lionel Fernel Gamarra [a], Andrea Laurato Sertié [a,*]

[a] Hospital Israelita Albert Einstein, São Paulo, SP, Brazil
[b] Department of Biochemistry, Escola Paulista de Medicina, Universidade Federal de São Paulo, São Paulo, Brazil
[c] Pontifícia Universidade Católica Do Paraná, Escola de Medicina, Laboratório de Bioinformática e Neurogenética, Curitiba, Paraná, Brazil
[d] Centro de Estudos Do Genoma Humano e Células Tronco, Instituto de Biociências, Universidade de São Paulo, São Paulo, Brazil

ARTICLE INFO

Keywords:
Stem cells from human exfoliated deciduous teeth (SHED)
SHED-Derived cortical organoids
2D and 3D structural analysis
Extracellular measurements of neuronal connectivity

ABSTRACT

Cortical organoids derived from human induced pluripotent stem cells (hiPSCs) represent a powerful *in vitro* experimental system to investigate human brain development and disease, often inaccessible to direct experimentation. However, despite steady progress in organoid technology, several limitations remain, including high cost and variability, use of hiPSCs derived from tissues harvested invasively, unexplored three-dimensional (3D) structural features and neuronal connectivity. Here, using a cost-effective and reproducible protocol as well as conventional two-dimensional (2D) immunostaining, we show that cortical organoids generated from hiPSCs obtained by reprogramming stem cells from human exfoliated deciduous teeth (SHED) recapitulate key aspects of human corticogenesis, such as polarized organization of neural progenitor zones with the presence of outer radial glial stem cells, and differentiation of superficial- and deep-layer cortical neurons and glial cells. We also show that 3D bioprinting and magnetic resonance imaging of intact cortical organoids are alternative and complementary approaches to unravel critical features of the 3D architecture of organoids. Finally, extracellular electrical recordings in whole organoids showed functional neuronal networks. Together, our findings suggest that SHED-derived cortical organoids constitute an attractive model of human neurodevelopment, and support the notion that a combination of 2D and 3D techniques to analyze organoid structure and function may help improve this promising technology.

1. Introduction

The expansion in size and complexity of the human cerebral cortex is thought to have enabled the evolutionary development of human cognition and language (Rakic 2009; Lui et al., 2011). However, this complexity might have also increased the vulnerability of the human brain to neuropsychiatric disorders that have their roots in neurodevelopment. Although studies using human fetal brain tissue and model organisms, especially rodents, have advanced our current knowledge of brain development and disease (Hirotsune et al., 1998; Pollen et al., 2015; Eze et al., 2021; Di Bella et al., 2021), there is an outstanding demand for experimental systems that closely mimic human cortical development and are also accessible and ethically appropriate (Zhao and Bhattacharyya, 2018).

Human induced pluripotent stem cell (hiPSC)-derived brain organoids have emerged as a powerful experimental platform to uncover the complex process of human brain development (Di Lullo and Kriegstein, 2017; Kelley and Pașca, 2022). It has been shown that organoids can reproduce early human brain organogenesis in terms of developmental trajectories, cellular composition, architectural features, transcriptional

* Corresponding author. Centro de Ensino e Pesquisa Albert Einstein, Rua Comendador Elias Jafet, 755. Morumbi – São Paulo, CEP, 05653-000, Brazil.
E-mail address: andrea.sertie@einstein.br (A.L. Sertié).
[1] These authors contributed equally to this work and should be considered joint first authors.

https://doi.org/10.1016/j.neuint.2024.105854
Received 22 December 2023; Received in revised form 2 September 2024; Accepted 2 September 2024
Available online 4 September 2024

and epigenetic profiles, and electrical activity (Paşca et al., 2015; Camp et al., 2015; Luo et al., 2016; Birey et al., 2017; Quadrato et al., 2017; Trujillo et al., 2019; Velasco et al., 2019; Trevino et al., 2020; Uzquiano et al., 2022). In addition, as hiPSC-derived brain organoids maintain the human genomic context, they have been applied to capture the pathogenesis of several genetic and environmentally related brain disorders (Lancaster et al., 2013; Mariani et al., 2015; Li et al., 2017; Velasco et al., 2020; Paulsen et al., 2022; Dwivedi et al., 2023).

Over the past few years, a variety of protocols have been described and refined for the generation of brain organoids (Di Lullo and Kriegstein, 2017). Although most studies have focused on modeling cortical development (Paşca et al., 2015; Mariani et al., 2015; Qian et al., 2016; Velasco et al., 2019), a number of other region-specific brain organoids (Zhong et al., 2014; Sakaguchi et al., 2015; Qian et al., 2016; Monzel et al., 2017; Birey et al., 2017) and assembloids (Birey et al., 2017; Xiang et al., 2017; Bagley et al., 2017; Sloan et al., 2018) have been described. Despite these advances, there are still many methodological challenges to be addressed, including costs and reproducibility, generation of brain organoids from hiPSCs obtained from easily accessible tissues, and 3D structural analysis and measurements of neuronal activity.

In this study, using a relatively simple guided protocol, we aimed to generate cortical organoids from hiPSCs obtained by reprogramming stem cells from human exfoliated deciduous teeth (SHED), a readily accessible source of children's cells shown to be suitable for neurodevelopmental disease modeling using 2D cultures (Russo et al., 2018; Sánchez-Sánchez et al., 2018; Griesi-Oliveira et al., 2021; Teles e Silva et al., 2022), and investigate the effectiveness of alternative methods to analyze the structure of the entire organoids, such as 3D bioprinting and magnetic resonance imaging. Also, we performed extracellular recordings of spontaneous electrical activity from wholemount organoids using multielectrode arrays.

2. Materials and methods

2.1. Generation of cortical organoids

The hiPSC line used in the present study has been previously generated from SHED derived from a neurotypical male child (referred to as F5541-1) through retroviral transduction of vectors containing *SOX2*, *c-MYC*, *OCT4*, and *KLF4*, and has been reported to express pluripotency-associated markers, differentiate into cells of the three germ layers *in vitro*, and to successfully generate neural progenitor cells and neurons in 2D cultures (Griesi-Oliveira et al., 2021). It is also noteworthy that our experience demonstrates that cryostorage of both SHED and SHED-derived hiPSC lines for long periods has no major negative effect on stem cell quality and potency (Griesi-Oliveira et al., 2015; Suzuki et al., 2015; Griesi-Oliveira et al., 2018; Sánchez-Sánchez et al., 2018; Griesi-Oliveira et al., 2021; Teles e Silva et al., 2022).

To produce cortical organoids from this SHED-derived hiPSC line, we used the protocol described in (Sloan et al., 2018) with slight modifications, which we have recently adopted to produce well-structured dorsal forebrain organoids from urine-derived hiPSCs (Teles e Silva et al., 2023). This protocol allows sustained 3D suspension culture in standard incubators without embedding into extracellular matrices or the use of rotating bioreactors, which may provide accessible and affordable technology for brain organoid construction. Briefly, hiPSCs were grown on 60 mm culture dishes coated with vitronectin (0.5 μg/cm^2) until the colonies reached ~2.5 mm in diameter. Intact colonies were then lifted from the plates using dispase and transferred to ultra-low attachment 6-well plates to form neural spheroids (~7–10 spheroids per well, total of ~150 spheroids) and cultured in neural induction medium (NIM) supplemented with the two SMAD inhibitors dorsomorphin (5 μM) and SB-4321542 (10 μM), and the ROCK inhibitor Y-27632 (10 μM) (Day 0). From day 2 to day 5, neural spheroids were grown in NIM with dorsomorphin and SB-4321542, with daily medium changes. On day 6, the medium was replaced by neural differentiation medium (NDM) supplemented with bFGF (20 ng/ml) and EGF (20 ng/ml) until day 24, with medium changes every other day. Also, from day 6 onwards an orbital shaker was used to enhance nutrient and oxygen diffusion. From day 25 to day 43, cortical organoids were grown in NDM with BDNF (20 ng/ml) and NT3 (20 ng/ml), with medium changes every 2–3 days. From day 44 onwards, the medium was replaced by NDM without any growth factor, with medium changes every four days until cortical organoids were collected for analysis. Two independent rounds of organoid differentiation were performed. Experiments were conducted separately on batch 1 and/or batch 2 organoids as described in the Figure legends.

The Ethics Committee of the Hospital Israelita Albert Einstein approved all phases of this study, and written informed consent was obtained from the participant and his parents/legal guardians.

2.2. Bioink preparation and 3D bioprinting of cortical organoids

Bioink preparation, bioprinting, and crosslinking were prepared based on the protocol described in (Cruz et al., 2023). Briefly, a combination of sodium alginate (Alg) (Sigma-Aldrich) and gelatin from pork skin (Gel) (Sigma-Aldrich) was used for the bioink composition. Both Alg (6% w/v) and Gel (4% w/v) were dissolved in sterile phosphate-buffered saline (PBS), at 72 °C. On the 6th day of culture, neural spheroids (n = 3) were mixed with 1 ml of the bioink, transferred to a 5 ml syringe with a 22-gauge blunt needle, and placed in the printhead of a 3D bioprinter (Educational Starter Printer, 3D Biotechnology Solutions, 3DBS Brazil). Bioprinting was performed at room temperature, under G-code control, using an extrusion code. The bioprinted constructs were then carefully transferred to a petri dish and maintained under rotation in NDM supplemented with bFGF and EGF until day 25, with medium changes every other day, to promote the proliferation of neural progenitors and initiate corticogenesis.

2.3. Immunocytochemistry staining

Immunocytochemistry staining of sectioned organoid samples at days 30, 60, and 90 of differentiation (n = 2–3 organoids for each time point) was performed as described in (Teles e Silva et al., 2023). Briefly, whole organoids were fixed with 4% paraformaldehyde in PBS at 4 °C, submerged in 30% sucrose until they sink, transferred to cryogenic molds, embedded in OCT, and stored at −80 °C. Frozen organoids were sliced into 15 μm sections using a cryostat. For immunostaining, organoid sections were permeabilized/blocked in 5% donkey serum and 1% triton in PBS at room temperature for 1 h and then incubated with primary antibodies overnight at 4 °C. After PBS washings, organoid sections were incubated at room temperature for 1 h with secondary antibodies conjugated with AlexaFluor 594 or AlexaFluor 488. Nuclei were counter-stained with DAPI. Fluorescence images were obtained using a Zeiss LSM 710 confocal microscope system. For wholemount immunostaining of the bioprinted organoids at day 25 of differentiation (n = 3), wholemount organoids were immersed in 4% paraformaldehyde solution in PBS for 40 min at room temperature, washed with PBS to remove the bioink, and then the immunostaining procedure was conducted as described above. See the list of antibodies and their information in Table S1.

2.4. Measurements of organoid size, cellular density, and number of ventricular zone-like regions

The overall morphology of the non-printed and bioprinted organoids was assessed through bright-field image analysis (EVOS M5000 Imaging System), and the 2D surface area of the organoids was measured using ImageJ macro-toolsets (National Institutes of Health, USA, http://imagej.nih.gov/ij) (n = 20–150 organoids for each time point). To measure the cellular density within the cryosectioned organoids at day 30 of differentiation (n = 2 organoids, 3–4 VZ-/PP-like regions for each

organoid), DAPI-stained nuclei were counted using ImageJ Cell Counter plugin. Ventricular zone (VZ)-like structures were defined by polarized neuroepithelium-like formations arranged around a central lumen and the outer preplate-like layer was defined by the area outside of the VZ to the organoid edge. The DAPI channel was also used to manually count the number of VZ-like structures per organoid slice for each time point (n = 6 slices from 2 to 3 organoids for each time point).

2.5. Western blot analyses

Western blot analysis was performed as described in (Teles e Silva et al., 2023) using extracts from intact organoid samples at days 30, 60, and 90 of organoid differentiation (n = 2–3 organoids for each time point). Briefly, total protein extracts from whole organoids were obtained using RIPA Buffer and then were sonicated. The protein concentration of each lysate was determined using the Pierce BCA protein assay, and the Glomax® Discover Microplate Reader. For immunoblotting, total proteins (10–20 μg) were separated by SDS–PAGE (8–10%) and transferred to nitrocellulose membranes, which were then blocked and incubated overnight at 4 °C with primary antibodies (Table S1). Detection was performed using horseradish peroxidase–coupled anti-rabbit or anti-mouse secondary antibodies, ECL substrate, and the ChemiDoc MP Imaging System.

2.6. Magnetic resonance imaging (MRI)

To avoid movement during MRI data acquisition, organoids at days 30 and 90 (n = 4 organoids for each time point) were embedded in the bioink described above, transferred to a petri dish, and statically incubated for 6 h in NDM supplemented with bFGF and EGF. Organoid MR images were acquired over a period of 7.5 h on a Siemens Magnetom Prisma-Fit 3T MRI scanner equipped with a 64-channel head coil (software NUMARIS/4, version syngo MR E11). The images were obtained using 3D turbo spin-echo T1-weighted imaging sequences with generalized autocalibrating partially parallel acquisition (GRAPPA - factor PE of 2) under the following parameters: interleaved multi-slice mode, voxel size = 0.3 × 0.3 × 0.3 mm, slice thickness = 0.24 mm, TR = 1500 ms, TE = 123 ms, averages = 32, echo spacing = 12.3 ms, field of view (FOV) = 90 mm, echo trains per slice = 14, turbo factor = 15; flip angle = 120°, bandwidth = 220 Hz/Px, and acquisition time = 7.5 h. The assessment of organoid volume was performed using the Vitrea Advanced Visualization 7.14.4 Vital Canon. To measure the cellular density within the organoids after the MRI scans, whole organoids were fixed and washed to remove the bioink, cryosectioned, stained with DAPI, and analyzed using Image J, as described above (n = 2 organoids, 3–4 VZ-/PP-like regions for each organoid).

2.7. Microelectrode array (MEA)

Spontaneous extracellular field potentials in wholemount cortical organoids at day 90 of differentiation (n = 3) were acquired with a Multichannel MEA-2100 System for 120 electrodes, and data acquisition were performed using the Multi-Channel Suite package (Multi Channels Systems MCS GmbH). The analysis of MEA data was performed using MATLAB software and the toolbox MEA-ToolBox v1.151 (https://github.com/mirandarobbins/MEA-toolbox), based on the following parameters: High Pass Butterworth Filter (cutoff frequency, Hz) = 200, Filter Order (n) = 2, Sampling Frequency, Hz) = 20000), Baseline Noise Detection (baseline noise time window, ms) = 50, Pure Noise Time Window (s) = 2, Spike Detection (min. spike interval, ms) = 0, Min. Spike Amplitude (μs) = 0, Spike Detection Threshold (rms) = 5, Burst Detection (max interval) (start interval, s) = 0.17, Spike Number (n) = 10, Inter Burst Interval (s) = 0.3, Intra Burst Interval (s) = 0.2, Min. Burst Duration (s) = 0.01.

2.8. Statistical analysis

The results represent the mean ± SD of replicate determinations from one representative experiment of two independent experiments. Statistical analysis was performed using Graphpad Prism V8. The one-way ANOVA test and the Mann-Whitney *U* test were used to measure statistical significance. p values < 0.05 were considered statistically significant.

3. Results

3.1. Generation of cortical organoids from SHED-derived hiPSCs and characterization using 2D histological analysis

First, we examined whether SHED-derived hiPSCs could generate cortical organoids that recapitulate essential features of the human developing dorsal cerebral cortex using a guided, matrix- and spinning bioreactor-free protocol that enables efficient neuroectoderm formation and subsequent differentiation into various cell types that populate the neocortical layers (Sloan et al., 2018; Teles e Silva et al., 2023). We observed that the SHED-derived cortical organoids progressively grew in size during the first 8 weeks until they reach an average 2D surface area of ~4 mm^2 (Fig. 1A). By using conventional immunocytochemistry staining of cryosectioned organoids, we observed at the beginning of differentiation (day 30) an abundance of proliferative neural progenitor cells (NPCs) expressing SOX2, FOXG1, Nestin, and Ki67 that self-organized into polarized neuroepithelium-like structures, or ventricular zone (VZ)-like structures, resembling neural tubes. These structures were surrounded by a layer containing TBR2+ intermediate progenitors and MAP2+/SYN1-negative immature neurons reminiscent of the preplate (Fig. 1B–E). Notably, at this stage of organoid differentiation, the density of cells in the preplate-like layer was significantly smaller than in the VZ-like areas, where nuclei are elongated, densely packed, and radially aligned (Fig. 1C). Progressively (days 60 and 90), we observed a significant reduction of the VZ-like formations (Fig. 1D), and an increase in the proportion of MAP2+/SYN1+ mature neurons, and of lower TBR1+/CTIP2+ and upper SATB2+ cortical layer neurons (Fig. 1B–E). Also, we detected a population of SOX2+ HOPX + outer radial glial cells (oRGCs) above the VZ-like structures, a hallmark of embryonic human cerebral cortex primarily located in the outer subventricular zone (SVZ) (Pollen et al., 2015) (Fig. 1B–S1). At these stages, we also observed an increase in the proportion of $CD44^+$ and GFAP + astrocytes (Fig. 1B). It is also noteworthy that GABAergic parvalbumin + interneurons, which originate from ventral forebrain progenitors, were absent in organoids at day 90, further suggesting the dorsal forebrain identity of the organoids (data not shown). Finally, the spatiotemporal cellular composition of the cortical organoids generated from SHED-derived hiPSCs is comparable to those of cortical organoids produced through similar protocols from fibroblast-derived hiPSCs (Paşca et al., 2015; Sloan et al., 2018), the conventionally used starting material to produce brain organoids, and from urine-derived hiPSCs, another noninvasive source of somatic cells suitable for generating cortical organoids (Teles e Silva et al., 2023). These findings, therefore, suggest that the SHED-derived cortical organoids recapitulate some fundamental features of early human corticogenesis and represent a novel more accessible system to examine mechanisms of human brain development.

3.2. Alternative approaches to analyze the 3D structure of entire organoids

Next, we sought to verify the advantages and limitations and potential applications of alternative methods to analyze the 3D spatial information of intact organoids. As 3D bioprinting has emerged as a promising approach that enables the construction of precisely controlled 3D tissue structures (Murphy et al., 2020; Banerjee et al., 2022), we

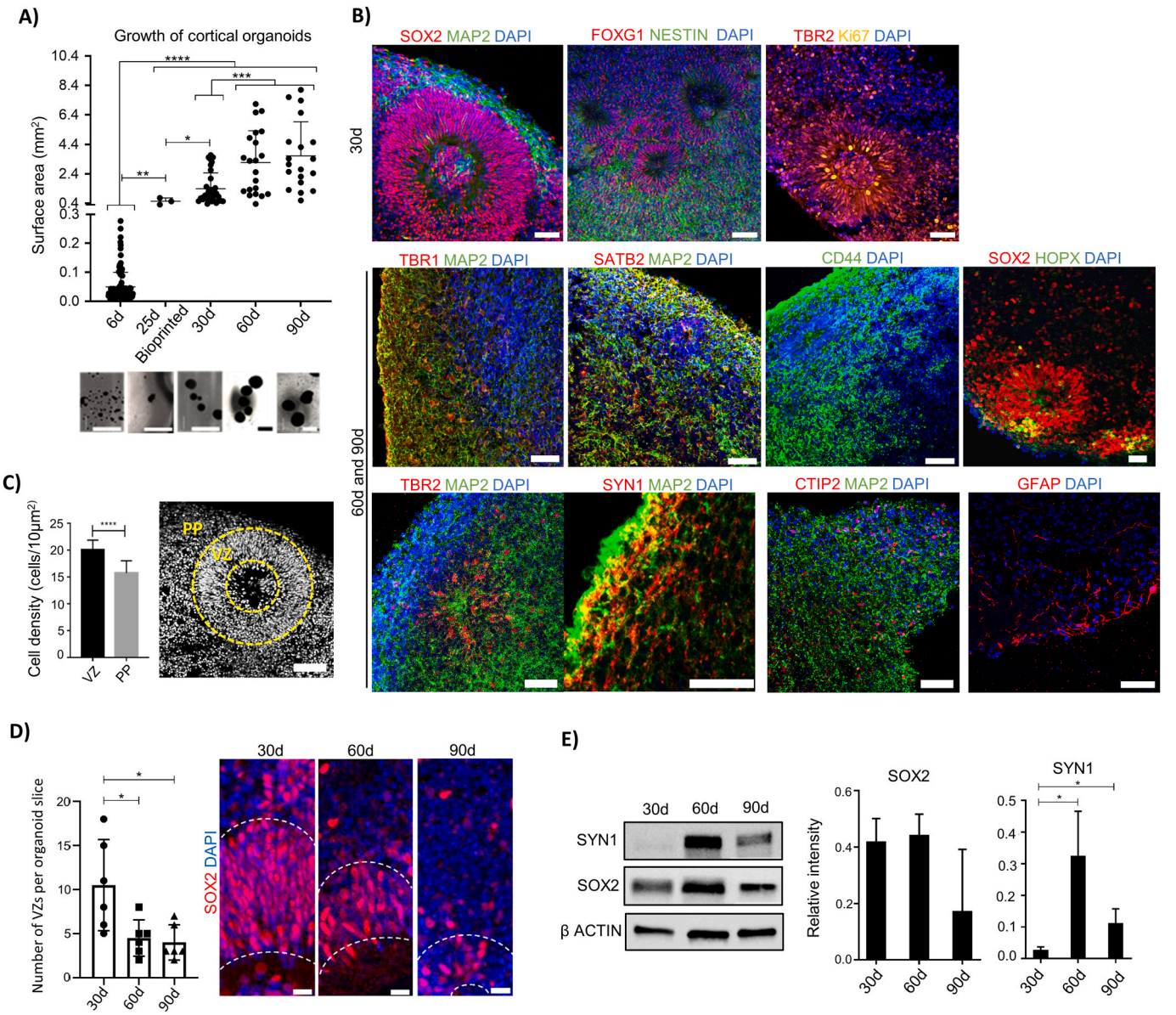

Fig. 1. Cortical organoids from SHED-derived hiPSCs recapitulate key aspects of human cortical development. (A) Graph showing the growth of cortical organoids (based on the average surface area, mm^2) at different stages of *in vitro* culture: days (d) 6, 30, 60, and 90 of differentiation. Data are presented as mean ± SEM (n = 20–150 organoids for each time point). The graph also shows the average surface area (mm^2) of bioprinted organoids at day 25 of differentiation (n = 3) (see section 3.2). Representative brightfield images of organoids taken at each time point are also presented. Scale bars, 2 mm. **(B)** Representative immunostainings of cortical organoids at days 30, 60, and 90 of differentiation (n = 2–3 organoids for each time point). At day 30, the organoids are composed of proliferating NPCs (SOX2, FOXG1, Nestin, and Ki67) self-organized into VZ-like structures surrounded by intermediate progenitors (TBR2) and immature neurons (MAP2). At days 60 and 90, the organoids exhibit mature neurons (MAP2 and SYN1), lower (TBR1 and CTIP2) and upper (SATB2) cortical layer neurons, and glial cells (CD44 and GFAP). At these stages, the organoids also exhibit a layer of outer radial glial cells (SOX2 and HOPX) above the VZ-like structures (SOX2). Nuclei are stained with DAPI (blue). Scale bars, 50 µm. While large necrotic cores were not observed in most high-quality slices of organoids that were selected for immunocytochemistry staining, the possibility of the formation of necrotic zones in the central part of some organoids as they grow in size was not analyzed and cannot be excluded. **(C)** Graph showing the cell density (cells/10 µm2) in the VZ- and preplate-like (PP) regions of cortical organoids at day 30. Data are presented as mean ± SEM (n = 2 organoids, 3–4 VZ-/PP-like regions for each organoid). A representative image of DAPI-stained nuclei in the VZ-/PP-like regions of an organoid at day 30 is also presented. Dashed lines indicate the borders of VZ-like structures. Scale bars, 50 µm. **(D)** Graph showing the number of VZ-like structures per organoid slice. Data are presented as mean ± SEM (n = 6 slices from 2 to 3 organoids for each time point). Representative images of SOX2-stained NPCs of cortical organoids at days 30, 60, and 90 showing the reduction in VZ-like structure size during culture time are also presented. Nuclei are stained with DAPI (blue). Dashed lines indicate the borders of VZ-like structures. Scale bars, 25 µm. **(E)** Representative immunoblot images showing the expression patterns of neural progenitor (SOX2) and neuron (SYN1) markers over the course of cortical organoid development. Graphs show mean SOX2 and SYN1 expression levels (±SEM) (n = 3 organoids for each time point). $p < 0.05$, $^{**}p \leq 0.01$, $^{***}p \leq 0.001$, $^{****}p \leq 0.0001$. Experiments were conducted separately on batch 1 and batch 2 organoids and similar results were obtained. The data presented are from one representative batch of differentiation. (For interpretation of the references to colour in this figure legend, the reader is referred to the Web version of this article.)

assessed the ability of bioprinted cortical organoids to maintain cytoarchitectural features resembling the early developing cortex. Using a bioink formulation composed of sodium alginate and gelatin, SHED-derived neural spheroids on the 6th day of culture were bioprinted, transferred to a petri dish, and maintained under rotation in neural differentiation medium until the 25th day of culture (Fig. 2A). We observed that the sphere-shaped bioprinted organoids exhibited significantly reduced growth compared to non-printed organoids at the same stage of differentiation (Fig. 1A), which could be attributed to mechanical properties of the bioink, such as stiffness and porosity, and also a shortage of nutrients and oxygen. Despite this, wholemount immunostaining of bioprinted organoids allowed simultaneous visualization of several well-defined VZ-like structures with packed SOX2+ NPCs surrounded by MAP2+ neurons (Fig. 2B). Therefore, these results suggest that this bioink composition provides a suitable environment for early neurogenesis with defined organization, and also that immunostaining of whole bioprinted organoids allows the analysis of the 3D spatial distribution of VZ-like areas and adjacent neuronal layers at the organoid surface. These initial findings have the potential to pave the way for construction of more complex organoid structures.

Magnetic resonance imaging (MRI) is a 3D imaging technique that has been extensively used to non-invasively examine the anatomy and pathology of the brain *in vivo* (Talos et al., 2006; Lerch et al., 2017). However, its application to brain organoid studies is still largely unexplored. Therefore, we next analyzed the feasibility and utility of MRI to explore structural features of the SHED-derived cortical organoids at early (30 days) and late (90 days) stages of development. For MRI data acquisition, organoids were encapsulated in the sodium alginate-gelatin bioink to reduce movement and scanned over 7.5 h using a 3T MRI machine (Fig. 3A). Representative T1-weighted images are shown in Fig. 3B, and the fifth image of each panel was then selected for further structural description. We observed that the organoid at day 30 (with a volume of 2.88 mm^3) showed hypointense areas highlighted with green as well as hyperintense regions highlighted with yellow-orange, and the organoid at day 90 (with a volume of 17.11 mm^3) exhibited almost exclusively hypointense blue-green areas. Importantly, while the hyperintense signals appeared to correlate with areas of higher cellularity, such as VZ-like structures, the hypointense signals appeared to indicate decreased cellularity, revealed by DAPI nuclear staining of the same sectioned organoids (Fig. 3B–D). These results highlight the potential of using MRI to unravel some aspects of the 3D architecture of cortical organoids.

3.3. Microelectrode array (MEA) to analyze the functionality of entire organoids

Characterizing the electrophysiological activity of human cortical organoids is key to ensure their relevance in physiological and pathological processes. Therefore, in addition to the analysis of the structure of the SHED-derived organoids, we interrogated the presence of spontaneous network activity in these organoids at a late developmental time point, day 90 of differentiation, by using a 120-channel MEA platform. We found that the majority of the channels containing organoids exhibited spontaneous electrical activity which could be measured by biocomputational analysis over different time intervals (Fig. S2). Representative recordings from a MEA channel are shown in Fig. 4. We observed high-frequency sequences of action potentials (spike trains) grouped in bursts (Fig. 4A). We observed high-frequency sequences of action potentials (spike trains) grouped in bursts (Fig. 4A). A detailed analysis of the burst activity over a 0.1-s interval showed organized temporal spike-train patterns (Fig. 4B) with relatively regular intervals between bursts (Fig. 4C), suggesting the presence of synchronized electrical activity (Pasquale et al., 2010). In addition, the interspike interval (ISI) analysis, which measure the period of inactivity between pikes, showed that the distribution of ISIs ranged from 0.01 to 0.05 s (Fig. 4D), also supporting the presence of non-random spiking dynamics. Finally, the single-channel burst (SCB) analysis over a 0.1-s interval also revealed that the organoid exhibited a collection of consecutive spikes with small ISIs (Fig. 4E). These data indicate that the SHED-derived organoids show intrinsic neuronal network activity, an important

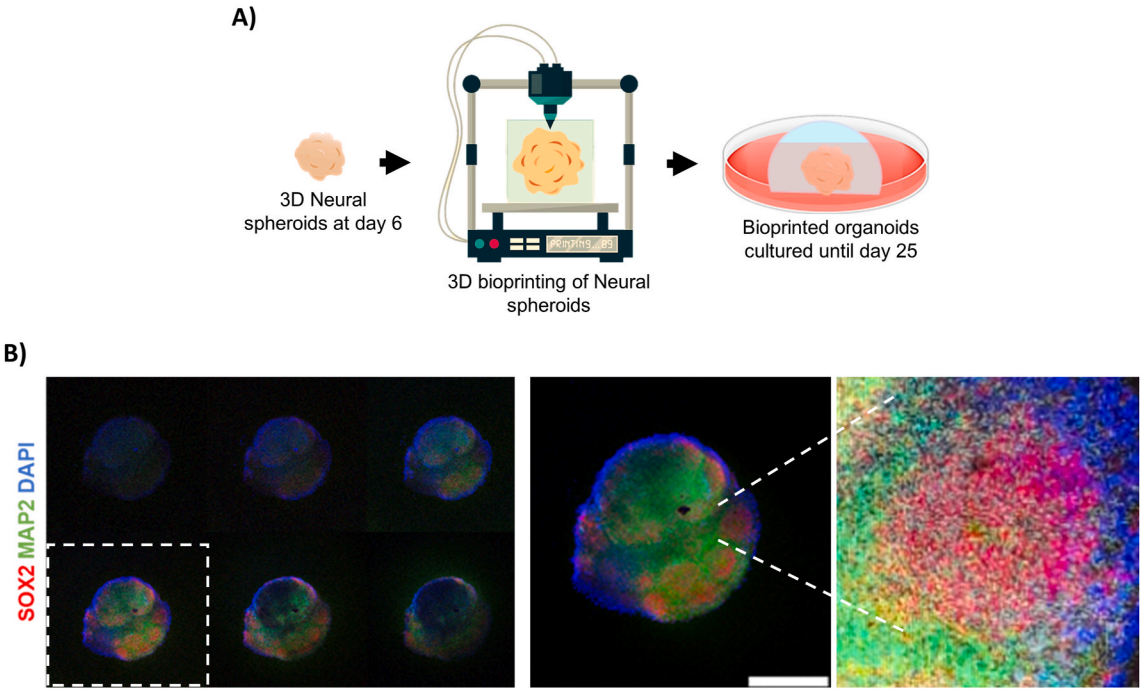

Fig. 2. 3D-bioprinted SHED-derived cortical organoids exhibit multiple VZ-like structures. (A) Schematic diagram illustrating the major steps of the cortical organoid bioprinting process. **(B)** Representative sequential confocal images of wholemount immunostainings of a bioprinted cortical organoid at day 25 of differentiation showing multiple VZ-like structures with packed SOX2 NPCs surrounded by MAP2 neurons (n = 3 organoids from one batch). Nuclei are stained with DAPI (blue). Scale bars, 400 μm. (For interpretation of the references to colour in this figure legend, the reader is referred to the Web version of this article.)

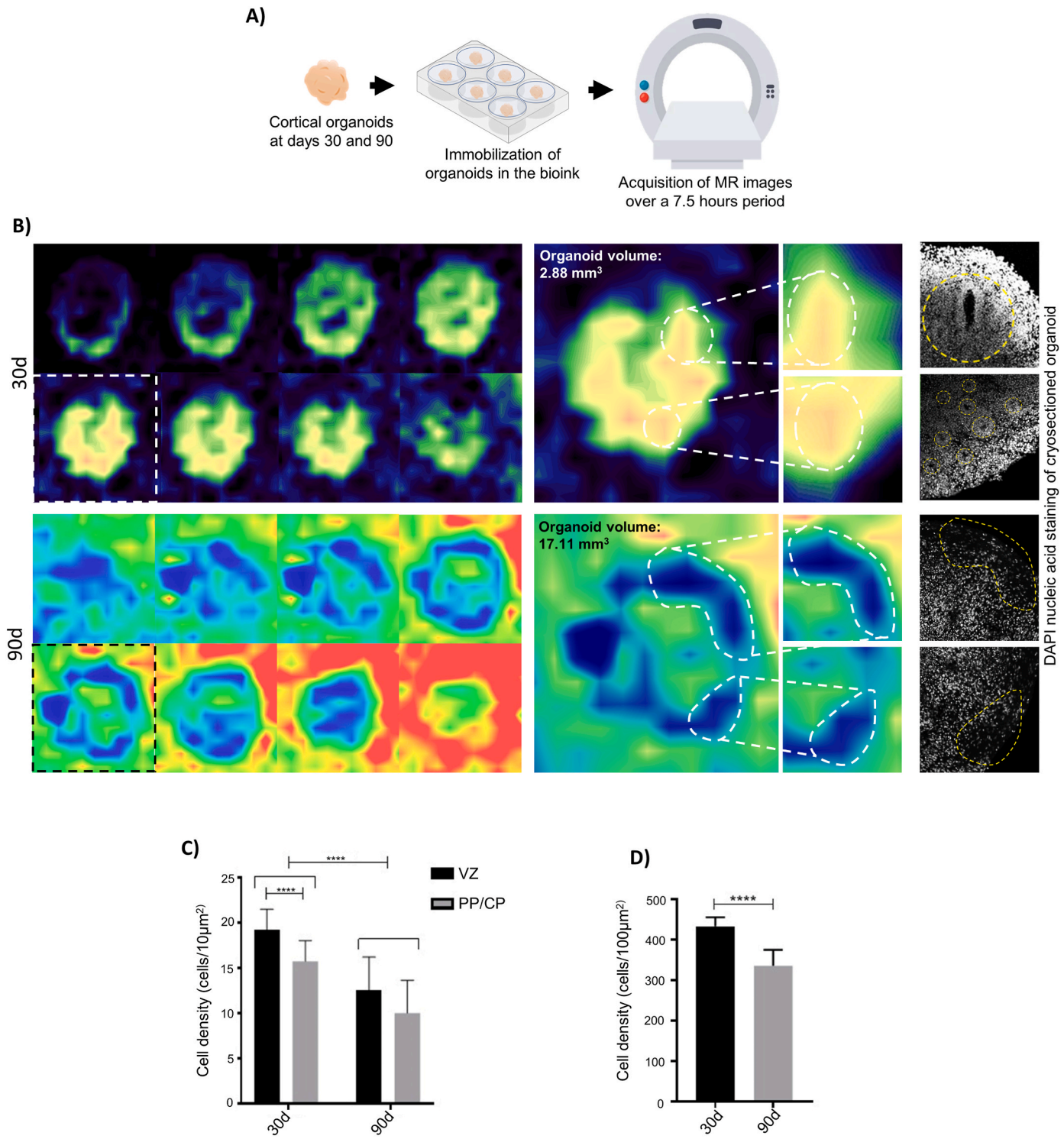

Fig. 3. Magnetic resonance imaging of SHED-derived cortical organoids reveals aspects of the 3D architecture of organoids. (A) Schematic diagram illustrating the major steps for MRI of cortical organoids. **(B)** Representative T1-weighted images of organoids at days 30 and 90 (n = 4 organoids for each time point). The fifth image of each panel was magnified for further description. The organoids, with volumes of 2.88 mm^3 and 17.11 mm^3 respectively, exhibit hypointense signals (blue-green) which appear to correlate with areas of decreased cellularity, and hyperintense signals (yellow-orange) which appear to correlate with regions of higher cellularity, such as VZ-like structures, revealed by DAPI nuclear staining of the same sectioned organoids (in grayscale). Dashed lines indicate the borders of areas with high cell density within the organoid at day 30 and borders of areas with low cell density within the organoid at day 90. **(C)** Graph showing the cell density (cells/10 µm2) in the VZ- and preplate-like (PP) regions of cortical organoids at day 30 and cortical plate-like (CP) regions of cortical organoids at day 90 after the MRI. Data are presented as mean ± SEM (n = 2 organoids for each time point, 3–4 VZ-/PP-/CP-like regions for each organoid). **(D)** Graph showing the cell density (cells/100 µm2) outside the VZ- and PP-/CP-like regions of cortical organoids at days 30 and 90 after the MRI. Data are presented as mean ± SEM (n = 2 organoids for each time point). ****$p \leq 0.0001$. Experiments were conducted separately on batch 1 and batch 2 organoids and similar results were obtained. The data presented are from one representative batch of differentiation. (For interpretation of the references to colour in this figure legend, the reader is referred to the Web version of this article.)

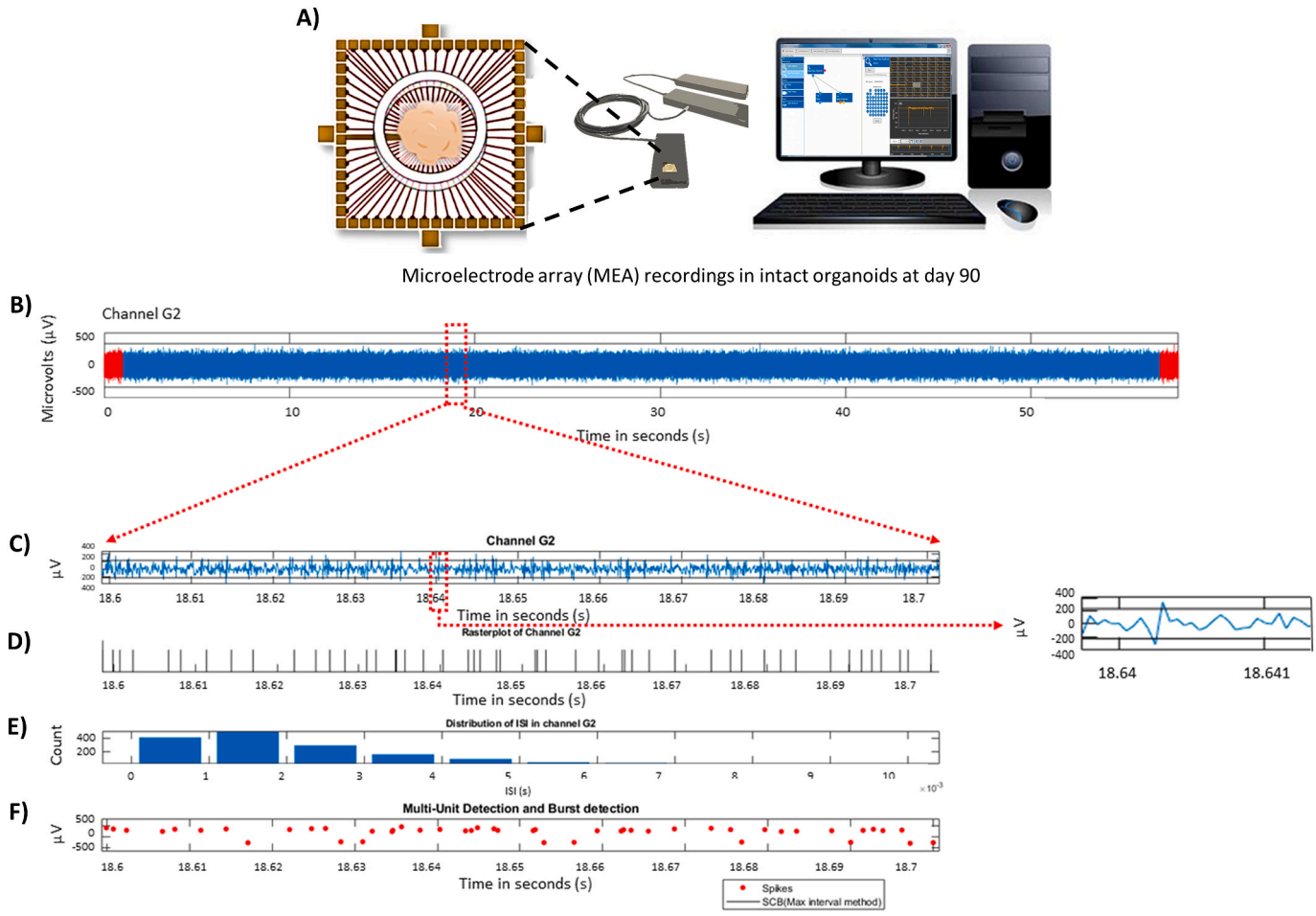

Fig. 4. Cortical organoids from SHED-derived hiPSCs show functional neuronal networks. (A) Schematic illustration of electrophysiological recordings of intact organoids at day 90 with the MEA-2100 System. **(B)** Representative MEA recordings (MEA channel G2) showing a 60-s interval of spiking activity across the organoid (n = 3 organoids from one batch). **(C)** Detailed analysis of the burst activity over a 0.1-s interval (channel G2, interval 18.6–18.7 s) showing the distribution of spikes within the bursts. The arrow indicates a single burst (channel G2, interval 18.640–18.641 s). **(D)** Spike raster plot depicting electrical activities derived from the organoid (channel G2, interval 18.6–18.7 s). Bursts are represented by thin vertical lines. **(E)** Histogram showing the number of interspike intervals (ISI) falling into each time bin (channel G2). The distribution of ISIs ranged from 0.01 to 0.05 s. **(F)** Single-channel burst (SCB) analysis showing a collection of consecutive spikes with small ISIs (channel G2, interval 18.6–18.7 s).

characteristic feature of the developing cortex.

4. Discussion

In this study, using a relatively simple and reproducible protocol as well as conventional 2D histology, we show that SHED-derived hiPSCs can reliably generate cortical organoids with similar developmental trajectories of the embryonic human cortex. Specially, these organoids exhibit well-structured VZ- and SVZ-like formations with a distinct human-specific outer radial glial cell layer, neuronal subtypes found in upper- and lower cortical layers, and also glial cells. SHED comprises a population of postnatal stem cells capable of extensive proliferation and multilineage differentiation that can be easily and noninvasively collected from children (Miura et al., 2003; Victor and Reiter, 2017). Previous studies using both undifferentiated SHED and SHED-derived neuronal and glial cells in 2D cultures have proven their suitability for modeling neurodevelopmental disorders, such as autism spectrum disorder (Griesi-Oliveira et al., 2015; Suzuki et al., 2015; Russo et al., 2018; Griesi-Oliveira et al., 2018; Sánchez-Sánchez et al., 2018; Griesi-Oliveira et al., 2021; Teles e Silva et al., 2022), Angelman syndrome (Urraca et al., 2018), 15q duplication syndrome (Dunaway et al., 2017; Urraca et al., 2018), Rett syndrome (Hirofuji et al., 2018), and Down syndrome (Pham et al., 2018; Sun et al., 2022). Thus, the SHED-derived cortical organoids reported here constitute an easily accessible platform to investigate molecular and cellular processes underlying early human brain development and dysfunction in a more physiologically 3D relevant context.

Currently, conventional immunostaining against cell-type-specific markers on cryosectioned brain organoids has been the mainly employed methodology to explore the structural organization of organoids (Paşca et al., 2015; Mariani et al., 2015; Qian et al., 2016), and only a few studies have assessed the 3D spatial information of intact organoids (Albanese et al., 2020; Ma et al., 2022; Yildirim et al., 2022). Therefore, alternative strategies for 3D analysis of entire brain organoids are needed to help improving their characterization and applications. Here, we show the ability of 3D bioprinted hiPSC-derived neural spheroids to generate cortical organoids with multiple VZ-like structures whose superficial localization can be visualized by whole-mount immunofluorescence staining of organoids. Although the bioink used for organoid bioprinting inhibited organoid growth over time and requires improvements, it may mimic mechanical forces arising from the extracellular matrix that are important for proper brain development (Javier-Torrent et al., 2021). Also, we observed that its alginate-gelatin-based composition maintained organoid sphericity and supported VZ organization and neurogenesis within organoids. In agreement with these findings, previous studies have shown that bioinks

with alginate, a naturally occurring polysaccharide, maintain human NPC stemness and also enable their differentiation into neurons, with neuronal cell clusters interconnected by neurites (Gu et al., 2016; Cruz et al., 2023). The application of 3D bioprinting to NPCs and brain organoids is a field in its infancy and can facilitate the fabrication of reproducible brain-like tissue constructs with precise biomechanical properties and spatial architecture.

We also provide initial evidence that 3T MRI, a radiation-free procedure that uses magnets and radio waves to provide noninvasive and nondestructive anatomical images of soft tissues and organs *in vivo*, can also be a suitable approach to unravel some structural features of entire cortical organoids *in vitro*. While the images obtained needed higher resolution, they provided information on organoid volume and cellular density. Notably, some VZ-like structures, which host a dense population of progenitor cells, seem to appear as areas of high signal intensity in the organoids at day 30 of differentiation. Interestingly, a recent study has applied a 7T MRI scanner, which provides images with greater resolution than the routine 3T MRI scanners, to successfully monitor the graft position, growth, and volume of hiPSC-derived cortical organoids transplanted into the somatosensory cortex of newborn immunocompromised rats (Revah et al., 2022). It would be important to verify whether this approach is useful for detecting additional information on the organoid 3D organization.

Several studies measuring the electrophysiological properties of brain organoids have performed recordings from individual neurons (Paşca et al., 2015; Birey et al., 2017; Quadrato et al., 2017), which sacrifice functional information at the network level. By analyzing extracellular potentials from a relatively large array of electrodes simultaneously, MEAs have been increasingly adopted to examine the electrophysiological and neural network features of brain organoids, which can provide insights into the maturation and healthiness of organoids (Trujillo et al., 2019; Fair et al., 2020; Kathuria et al., 2020). Here, using a 120-channel MEA system, we show that SHED-derived cortical organoids exhibit spontaneous spike-firing and coordinated neuronal bursting activity, suggesting that these organoids are capable of forming organized neuronal networks. Interestingly, the patterns of electrical activity in the SHED-derived cortical organoids resemble those from a previous study that reported similarities between the electrophysiological properties of human fibroblast-derived cortical organoids and human preterm neonatal electroencephalogram (Trujillo et al., 2019).

Taken altogether, our results demonstrate the suitability of SHED-derived cortical organoids for structural and functional modeling of early stages of human brain development, as well as the utility of 2D and 3D techniques to analyze organoid properties, which may help address human-specific features of neurodevelopmental diseases.

CRediT authorship contribution statement

André Luíz Teles e Silva: Writing – original draft, Validation, Methodology, Investigation, Formal analysis. **Bruno Yukio Yokota-Moreno:** Writing – original draft, Validation, Methodology, Investigation, Formal analysis. **Mariana Silva Branquinho:** Validation, Methodology, Investigation, Formal analysis. **Geisa Rodrigues Salles:** Validation, Methodology, Investigation, Formal analysis. **Thiago Cattuzo de Souza:** Validation, Methodology, Investigation, Formal analysis. **Ronald Almeida de Carvalho:** Validation, Methodology, Investigation, Formal analysis. **Gabriel Batista:** Validation, Methodology, Investigation, Formal analysis. **Elisa Varella Branco:** Validation, Methodology. **Karina Griesi-Oliveira:** Validation, Methodology, Investigation, Formal analysis. **Maria Rita Passos Bueno:** Conceptualization. **Marimélia Aparecida Porcionatto:** Conceptualization. **Roberto Hirochi Herai:** Writing – original draft, Validation, Methodology, Formal analysis, Conceptualization. **Lionel Fernel Gamarra:** Writing – original draft, Validation, Methodology, Investigation, Formal analysis, Conceptualization. **Andrea Laurato Sertié:** Writing – review & editing, Supervision, Resources, Project administration, Funding acquisition, Conceptualization.

Declaration of competing interest

None.

Data availability

Data will be made available on request.

Acknowledgments

This research was funded by The State of Sao Paulo Research Foundation (FAPESP) grant number 2021/14491-2. We are grateful to all the individuals who participated in this work and their parents/legal guardians. We thank Natalia Torres, Raimundo Machado de Azevedo Neto, Vanessa Gil Salvatierra, Isabella de Sousa Nobrega, Karina Fernandes Dias Correa, and Alda Fernandes de Castro for technical assistance.

Appendix A. Supplementary data

Supplementary data to this article can be found online at https://doi.org/10.1016/j.neuint.2024.105854.

References

Albanese, A., Swaney, J.M., Yun, D.H., Evans, N.B., Antonucci, J.M., Velasco, S., Sohn, C. H., Arlotta, P., Gehrke, L., Chung, K., 2020. Multiscale 3D phenotyping of human cerebral organoids. Sci. Rep. 10 (1), 21487.

Bagley, J.A., Reumann, D., Bian, S., Lévi-Strauss, J., Knoblich, J.A., 2017. Fused cerebral organoids model interactions between brain regions. Nat. Methods 14 (7), 743–751.

Banerjee, D., Singh, Y.P., Datta, P., Ozbolat, V., O'Donnell, A., Yeo, M., Ozbolat, I.T., 2022. Strategies for 3D bioprinting of spheroids: a comprehensive review. Biomaterials 291, 121881.

Birey, F., Andersen, J., Makinson, C.D., Islam, S., Wei, W., Huber, N., Fan, H.C., Metzler, K.R.C., Panagiotakos, G., Thom, N., O'Rourke, N.A., Steinmetz, L.M., Bernstein, J.A., Hallmayer, J., Huguenard, J.R., Paşca, S.P., 2017. Assembly of functionally integrated human forebrain spheroids. Nature 545 (7652), 54–59.

Camp, J.G., Badsha, F., Florio, M., Kanton, S., Gerber, T., Wilsch-Bräuninger, M., Lewitus, E., Sykes, A., Hevers, W., Lancaster, M., Knoblich, J.A., Lachmann, R., Pääbo, S., Huttner, W.B., Treutlein, B., 2015. Human cerebral organoids recapitulate gene expression programs of fetal neocortex development. Proc. Natl. Acad. Sci. U.S. A. 112 (51), 15672–15677.

Cruz, E.M., Machado, L.S., Zamproni, L.N., Bim, L.V., Ferreira, P.S., Pinto, L.A., Pessan, L. A., Backes, E.H., Porcionatto, M.A., 2023. A gelatin methacrylate-based hydrogel as a potential bioink for 3D bioprinting and neuronal differentiation. Pharmaceutics 15 (2), 627.

Di Bella, D.J., Habibi, E., Stickels, R.R., Scalia, G., Brown, J., Yadollahpour, P., Yang, S. M., Abbate, C., Biancalani, T., Macosko, E.Z., Chen, F., Regev, A., Arlotta, P., 2021. Molecular logic of cellular diversification in the mouse cerebral cortex. Nature 595 (7868), 554–559.

Di Lullo, E., Kriegstein, A.R., 2017. The use of brain organoids to investigate neural development and disease. Nat. Rev. Neurosci. 18 (10), 573–584.

Dunaway, K., Goorha, S., Matelski, L., Urraca, N., Lein, P.J., Korf, I., Reiter, L.T., LaSalle, J.M., 2017. Dental pulp stem cells model early life and imprinted DNA methylation patterns. Stem Cell. 35 (4), 981–988.

Dwivedi, I., Caldwell, A.B., Zhou, D., Wu, W., Subramaniam, S., Haddad, G.G., 2023. Methadone alters transcriptional programs associated with synapse formation in human cortical organoids. Transl. Psychiatry 13 (1), 151.

Eze, U.C., Bhaduri, A., Haeussler, M., Nowakowski, T.J., Kriegstein, A.R., 2021. Single-cell atlas of early human brain development highlights heterogeneity of human neuroepithelial cells and early radial glia. Nat. Neurosci. 24 (4), 584–594.

Fair, S.R., Julian, D., Hartlaub, A.M., Pusuluri, S.T., Malik, G., Summerfied, T.L., Zhao, G., Hester, A.B., Ackerman, WE 4th, Hollingsworth, E.W., Ali, M., McElroy, C. A., Buhimschi, I.A., Imitola, J., Maitre, N.L., Bedrosian, T.A., Hester, M.E., 2020. Electrophysiological maturation of cerebral organoids correlates with dynamic morphological and cellular development. Stem Cell Rep. 15 (4), 855–868.

Griesi-Oliveira, K., Acab, A., Gupta, A.R., Sunaga, D.Y., Chailangkarn, T., Nicol, X., Nunez, Y., Walker, M.F., Murdoch, J.D., Sanders, S.J., Fernandez, T.V., Ji, W., Lifton, R.P., Vadasz, E., Dietrich, A., Pradhan, D., Song, H., Ming, G.L., Gu, X., Haddad, G., Marchetto, M.C., Spitzer, N., Passos-Bueno, M.R., State, M.W., Muotri, A.R., 2015. Modeling non-syndromic autism and the impact of TRPC6 disruption in human neurons. Mol. Psychiatr. 20 (11), 1350–1365.

Griesi-Oliveira, K., Fogo, M.S., Pinto, B.G.G., Alves, A.Y., Suzuki, A.M., Morales, A.G., Ezquina, S., Sosa, O.J., Sutton, G.J., Sunaga-Franze, D.Y., Bueno, A.P., Seabra, G.,

Sardinha, L., Costa, S.S., Rosenberg, C., Zachi, E.C., Sertie, A.L., Martins-de-Souza, D., Reis, E.M., Voineagu, I., Passos-Bueno, M.R., 2021. Transcriptome of iPSC-derived neuronal cells reveals a module of co-expressed genes consistently associated with autism spectrum disorder. Mol. Psychiatr. 26 (5), 1589–1605.
Griesi-Oliveira, K., Suzuki, A.M., Alves, A.Y., Mafra, A.C.C.N., Yamamoto, G.L., Ezquina, S., Magalhães, Y.T., Forti, F.L., Sertie, A.L., Zachi, E.C., Vadasz, E., Passos-Bueno, M.R., 2018. Actin cytoskeleton dynamics in stem cells from autistic individuals. Sci. Rep. 8 (1), 11138.
Gu, Q., Tomaskovic-Crook, E., Lozano, R., Chen, Y., Kapsa, R.M., Zhou, Q., Wallace, G.G., Crook, J.M., 2016. Functional 3D neural mini-tissues from printed gel-based bioink and human neural stem cells. Adv. Healthcare Mater. 5 (12), 1429–1438.
Hirofuji, S., Hirofuji, Y., Kato, H., Masuda, K., Yamaza, H., Sato, H., Takayama, F., Torio, M., Sakai, Y., Ohga, S., Taguchi, T., Nonaka, K., 2018. Mitochondrial dysfunction in dopaminergic neurons differentiated from exfoliated deciduous tooth-derived pulp stem cells of a child with Rett syndrome. Biochem. Biophys. Res. Commun. 498 (4), 898–904.
Hirotsune, S., Fleck, M.W., Gambello, M.J., Bix, G.J., Chen, A., Clark, G.D., Ledbetter, D. H., McBain, C.J., Wynshaw-Boris, A., 1998. Graded reduction of Pafah1b1 (Lis1) activity results in neuronal migration defects and early embryonic lethality. Nat. Genet. 19 (4), 333–339.
Javier-Torrent, M., Zimmer-Bensch, G., Nguyen, L., 2021. Mechanical forces orchestrate brain development. Trends Neurosci. 44 (2), 110–121.
Kathuria, A., Lopez-Lengowski, K., Jagtap, S.S., McPhie, D., Perlis, R.H., Cohen, B.M., Karmacharya, R., 2020. Transcriptomic landscape and functional characterization of induced pluripotent stem cell-derived cerebral organoids in schizophrenia. JAMA Psychiatr. 77 (7), 745–754.
Kelley, K.W., Pașca, S.P., 2022. Human brain organogenesis: toward a cellular understanding of development and disease. Cell 185 (1), 42–61.
Lancaster, M.A., Renner, M., Martin, C.A., Wenzel, D., Bicknell, L.S., Hurles, M.E., Homfray, T., Penninger, J.M., Jackson, A.P., Knoblich, J.A., 2013. Cerebral organoids model human brain development and microcephaly. Nature 501 (7467), 373–379.
Lerch, J.P., van der Kouwe, A.J., Raznahan, A., Paus, T., Johansen-Berg, H., Miller, K.L., Smith, S.M., Fischl, B., Sotiropoulos, S.N., 2017. Studying neuroanatomy using MRI. Nat. Neurosci. 20 (3), 314–326.
Li, Y., Muffat, J., Omer, A., Bosch, I., Lancaster, M.A., Sur, M., Gehrke, L., Knoblich, J.A., Jaenisch, R., 2017. Induction of expansion and folding in human cerebral organoids. Cell Stem Cell 20 (3), 385–396.e3.
Lui, J.H., Hansen, D.V., Kriegstein, A.R., 2011. Development and evolution of the human neocortex. Cell 146 (1), 18–36. Erratum in: Cell. 2011;146(2):332.
Luo, C., Lancaster, M.A., Castanon, R., Nery, J.R., Knoblich, J.A., Ecker, J.R., 2016. Cerebral organoids recapitulate epigenomic signatures of the human fetal brain. Cell Rep. 17 (12), 3369–3384.
Ma, H., Chen, J., Deng, Z., Sun, T., Luo, Q., Gong, H., Li, X., Long, B., 2022. Multiscale analysis of cellular composition and morphology in intact cerebral organoids. Biology 11 (9), 1270.
Mariani, J., Coppola, G., Zhang, P., Abyzov, A., Provini, L., Tomasini, L., Amenduni, M., Szekely, A., Palejev, D., Wilson, M., Gerstein, M., Grigorenko, E.L., Chawarska, K., Pelphrey, K.A., Howe, J.R., Vaccarino, F.M., 2015. FOXG1-Dependent dysregulation of GABA/glutamate neuron differentiation in autism spectrum disorders. Cell 162 (2), 375–390.
Miura, M., Gronthos, S., Zhao, M., Lu, B., Fisher, L.W., Robey, P.G., Shi, S., 2003. SHED: stem cells from human exfoliated deciduous teeth. Proc. Natl. Acad. Sci. U.S.A. 100 (10), 5807–5812.
Monzel, A.S., Smits, L.M., Hemmer, K., Hachi, S., Moreno, E.L., van Wuellen, T., Jarazo, J., Walter, J., Brüggemann, I., Boussaad, I., Berger, E., Fleming, R.M.T., Bolognin, S., Schwamborn, J.C., 2017. Derivation of human midbrain-specific organoids from neuroepithelial stem cells. Stem Cell Rep. 8 (5), 1144–1154.
Murphy, S.V., De Coppi, P., Atala, A., 2020. Opportunities and challenges of translational 3D bioprinting. Nat. Biomed. Eng. 4 (4), 370–380.
Pașca, A.M., Sloan, S.A., Clarke, L.E., Tian, Y., Makinson, C.D., Huber, N., Kim, C.H., Park, J.Y., O'Rourke, N.A., Nguyen, K.D., Smith, S.J., Huguenard, J.R., Geschwind, D.H., Barres, B.A., Pașca, S.P., 2015. Functional cortical neurons and astrocytes from human pluripotent stem cells in 3D culture. Nat. Methods 12 (7), 671–678.
Pasquale, V., Martinoia, S., Chiappalone, M., 2010. A self-adapting approach for the detection of bursts and network bursts in neuronal cultures. J. Comput. Neurosci. 29 (1–2), 213–229.
Paulsen, B., Velasco, S., Kedaigle, A.J., Pigoni, M., Quadrato, G., Deo, A.J., Adiconis, X., Uzquiano, A., Sartore, R., Yang, S.M., Simmons, S.K., Symvoulidis, P., Kim, K., Tsafou, K., Podury, A., Abbate, C., Tucewicz, A., Smith, S.N., Albanese, A., Barrett, L., Sanjana, N.E., Shi, X., Chung, K., Lage, K., Boyden, E.S., Regev, A., Levin, J.Z., Arlotta, P., 2022. Autism genes converge on asynchronous development of shared neuron classes. Nature 602 (7896), 268–273.
Pham, T.T.M., Kato, H., Yamaza, H., Masuda, K., Hirofuji, Y., Sato, H., Nguyen, H.T.N., Han, X., Zhang, Y., Taguchi, T., Nonaka, K., 2018. Altered development of dopaminergic neurons differentiated from stem cells from human exfoliated deciduous teeth of a patient with Down syndrome. BMC Neurol. 18 (1), 132.
Pollen, A.A., Nowakowski, T.J., Chen, J., Retallack, H., Sandoval-Espinosa, C., Nicholas, C.R., Shuga, J., Liu, S.J., Oldham, M.C., Diaz, A., Lim, D.A., Leyrat, A.A., West, J.A., Kriegstein, A.R., 2015. Molecular identity of human outer radial glia during cortical development. Cell 163 (1), 55–67.
Qian, X., Nguyen, H.N., Song, M.M., Hadiono, C., Ogden, S.C., Hammack, C., Yao, B., Hamersky, G.R., Jacob, F., Zhong, C., Yoon, K.J., Jeang, W., Lin, L., Li, Y., Thakor, J., Berg, D.A., Zhang, C., Kang, E., Chickering, M., Nauen, D., Ho, C.Y., Wen, Z., Christian, K.M., Shi, P.Y., Maher, B.J., Wu, H., Jin, P., Tang, H., Song, H., Ming, G.L., 2016. Brain-region-specific organoids using mini-bioreactors for modeling ZIKV exposure. Cell 165 (5), 1238–1254.
Quadrato, G., Nguyen, T., Macosko, E.Z., Sherwood, J.L., Min Yang, S., Berger, D.R., Maria, N., Scholvin, J., Goldman, M., Kinney, J.P., Boyden, E.S., Lichtman, J.W., Williams, Z.M., McCarroll, S.A., Arlotta, P., 2017. Cell diversity and network dynamics in photosensitive human brain organoids. Nature 545 (7652), 48–53.
Rakic, P., 2009. Evolution of the neocortex: a perspective from developmental biology. Nat. Rev. Neurosci. 10 (10), 724–735.
Revah, O., Gore, F., Kelley, K.W., Andersen, J., Sakai, N., Chen, X., Li, M.Y., Birey, F., Yang, X., Saw, N.L., Baker, S.W., Amin, N.D., Kulkarni, S., Mudipalli, R., Cui, B., Nishino, S., Grant, G.A., Knowles, J.K., Shamloo, M., Huguenard, J.R., Deisseroth, K., Pașca, S.P., 2022. Maturation and circuit integration of transplanted human cortical organoids. Nature 610 (7931), 319–326.
Russo, F.B., Freitas, B.C., Pignatari, G.C., Fernandes, I.R., Sebat, J., Muotri, A.R., Beltrão-Braga, P.C.B., 2018. Modeling the interplay between neurons and astrocytes in autism using human induced pluripotent stem cells. Biol. Psychiatr. 83 (7), 569–578.
Sakaguchi, H., Kadoshima, T., Soen, M., Narii, N., Ishida, Y., Ohgushi, M., Takahashi, J., Eiraku, M., Sasai, Y., 2015. Generation of functional hippocampal neurons from self-organizing human embryonic stem cell-derived dorsomedial telencephalic tissue. Nat. Commun. 6, 8896.
Sánchez-Sánchez, S.M., Magdalon, J., Griesi-Oliveira, K., Yamamoto, G.L., Santacruz-Perez, C., Fogo, M., Passos-Bueno, M.R., Sertié, A.L., 2018. Rare RELN variants affect Reelin-DAB1 signal transduction in autism spectrum disorder. Hum. Mutat. 39 (10), 1372–1383.
Sloan, S.A., Andersen, J., Pașca, A.M., Birey, F., Pașca, S.P., 2018. Generation and assembly of human brain region-specific three-dimensional cultures. Nat. Protoc. 13 (9), 2062–2085.
Sun, X., Kato, H., Sato, H., Han, X., Hirofuji, Y., Kato, T.A., Sakai, Y., Ohga, S., Fukumoto, S., Masuda, K., 2022. Dopamine-related oxidative stress and mitochondrial dysfunction in dopaminergic neurons differentiated from deciduous teeth-derived stem cells of children with Down syndrome. FASEB Bioadv 4 (7), 454–467.
Suzuki, A.M., Griesi-Oliveira, K., de Oliveira Freitas Machado, C., Vadasz, E., Zachi, E.C., Passos-Bueno, M.R., Sertie, A.L., 2015. Altered mTORC1 signaling in multipotent stem cells from nearly 25% of patients with nonsyndromic autism spectrum disorders. Mol. Psychiatr. 20 (5), 551–552.
Talos, I.F., Zou, K.H., Ohno-Machado, L., Bhagwat, J.G., Kikinis, R., Black, P.M., Jolesz, F.A., 2006. Supratentorial low-grade glioma resectability: statistical predictive analysis based on anatomic MR features and tumor characteristics. Radiology 239 (2), 506–513.
Teles e Silva, A.L., Glaser, T., Griesi-Oliveira, K., Corrêa-Velloso, J., Wang, J.Y.T., da, Silva Campos G., Ulrich, H., Balan, A., Zarrei, M., Higginbotham, E.J., Scherer, S. W., Passos-Bueno, M.R., Sertié, A.L., 2022. Rare CACNA1H and RELN variants interact through mTORC1 pathway in oligogenic autism spectrum disorder. Transl. Psychiatry 12 (1), 234.
Teles e Silva, A.L., Yokota, B.Y., Sertié, A.L., Zampieri, B.L., 2023. Generation of urine-derived induced pluripotent stem cells and cerebral organoids for modeling Down syndrome. Stem Cell. Rev. Rep 19 (4), 1116–1123.
Trevino, A.E., Sinnott-Armstrong, N., Andersen, J., Yoon, S.J., Huber, N., Pritchard, J.K., Chang, H.Y., Greenleaf, W.J., Pașca, S.P., 2020. Chromatin accessibility dynamics in a model of human forebrain development. Science 367 (6476), eaay1645.
Trujillo, C.A., Gao, R., Negraes, P.D., Gu, J., Buchanan, J., Preissl, S., Wang, A., Wu, W., Haddad, G.G., Chaim, I.A., Domissy, A., Vandenberghe, M., Devor, A., Yeo, G.W., Voytek, B., Muotri, A.R., 2019. Complex oscillatory waves emerging from cortical organoids model early human brain network development. Cell Stem Cell 25 (4), 558–569.e7.
Urraca, N., Hope, K., Victor, A.K., Belgard, T.G., Memon, R., Goorha, S., Valdez, C., Tran, Q.T., Sanchez, S., Ramirez, J., Donaldson, M., Bridges, D., Reiter, L.T., 2018. Significant transcriptional changes in 15q duplication but not Angelman syndrome deletion stem cell-derived neurons. Mol. Autism. 9, 6.
Uzquiano, A., Kedaigle, A.J., Pigoni, M., Paulsen, B., Adiconis, X., Kim, K., Faits, T., Nagaraja, S., Antón-Bolaños, N., Gerhardinger, C., Tucewicz, A., Murray, E., Jin, X., Buenrostro, J., Chen, F., Velasco, S., Regev, A., Levin, J.Z., Arlotta, P., 2022. Proper acquisition of cell class identity in organoids allows definition of fate specification programs of the human cerebral cortex. Cell 185 (20), 3770–3788.e27.
Velasco, S., Kedaigle, A.J., Simmons, S.K., Nash, A., Rocha, M., Quadrato, G., Paulsen, B., Nguyen, L., Adiconis, X., Regev, A., Levin, J.Z., Arlotta, P., 2019. Individual brain organoids reproducibly form cell diversity of the human cerebral cortex. Nature 570 (7762), 523–527.
Velasco, S., Paulsen, B., Arlotta, P., 2020. 3D brain organoids: studying brain development and disease outside the embryo. Annu. Rev. Neurosci. 43, 375–389.
Victor, A.K., Reiter, L.T., 2017. Dental pulp stem cells for the study of neurogenetic disorders. Hum. Mol. Genet. 26 (R2), R166–R171.
Xiang, Y., Tanaka, Y., Patterson, B., Kang, Y.J., Govindaiah, G., Roselaar, N., Cakir, B., Kim, K.Y., Lombroso, A.P., Hwang, S.M., Zhong, M., Stanley, E.G., Elefanty, A.G., Naegele, J.R., Lee, S.H., Weissman, S.M., Park, I.H., 2017. Fusion of regionally specified hPSC-derived organoids models human brain development and interneuron migration. Cell Stem Cell 21 (3), 383–398.e7.
Yildirim, M., Delepine, C., Feldman, D., Pham, V.A., Chou, S., Ip, J., Nott, A., Tsai, L.H., Ming, G.L., So, P.T.C., Sur, M., 2022. Label-free three-photon imaging of intact human cerebral organoids for tracking early events in brain development and deficits in Rett syndrome. Elife 11, e78079.
Zhao, X., Bhattacharyya, A., 2018. Human models are needed for studying human neurodevelopmental disorders. Am. J. Hum. Genet. 103 (6), 829–857.
Zhong, X., Gutierrez, C., Xue, T., Hampton, C., Vergara, M.N., Cao, L.H., Peters, A., Park, T.S., Zambidis, E.T., Meyer, J.S., Gamm, D.M., Yau, K.W., Canto-Soler, M.V.,

2014. Generation of three-dimensional retinal tissue with functional photoreceptors from human iPSCs. Nat. Commun. 5, 4047.